STATUS	TYPE	OCLC #
Conditions Accepted	Copy	931671993
SOURCE	**REQUEST DATE**	**NEED BEFORE**
ILLiad	03/20/2017	04/19/2017
BORROWER	**RECEIVE DATE**	**DUE DATE**
FTU		
LENDERS		
*UB#, UB#		

175142525

RN 181(55,1)

LOCAL ID RN 181(55,1) AIAA 2014-0109 gedr
AUTHOR

ARTICLE AUTHOR

TITLE 55th AIAA / : National Harbor, Maryland, USA, 13 - 17 January 2014; held at the AIAA SciTech Forum
IMPRINT Red Hook, NY Curran 2014

ISBN

ARTICLE TITLE Monitoring Strain Rate Effects on Nanocomposites using Piezospectroscopy
FORMAT
EDITION
VOLUME
NUMBER
DATE January 2014
PAGES 13-17

ALERT

VERIFIED <TN:732429><ODYSSEY:132.170.219.7/FTU>
MAX COST OCLC IFM - 30.00 USD
LEND CHARGES
LEND RESTRICTIONS

BORROWER NOTES Yes, airmail is fine.

AFFILIATION CRL/RAPID/Delivery/FLIN/SOLINE (SO6)
COPYRIGHT US:CCG

SHIPPED DATE
FAX NUMBER 407-823-3047 (fax) / 407-823-2383 (phone)
EMAIL illbor@ucf.edu / 132.170.217.20 (Odyssey)

ODYSSEY 132.170.219.7/FTU
ARIEL FTP
ARIEL EMAIL

BILL TO University of Central Florida
PO Box 162430 / ILL
12701 Pegasus Drive; Bldg 2
Orlando, FL, US 32816-2666

BILLING NOTES IFM preferred; Invoice OK

SHIP VIA Delivery / BOOK RATE / ODYSSEY/ MyBib eL®
SHIP TO University of Central Florida
PO Box 162430 - ILL
12701 Pegasus Drive; Bldg 2
Orlando, FL, US 32816-2666

RETURN VIA
RETURN TO

EILAUFTRAG

WICHTIGER HINWEIS

Alle Seiten mit Abbildungen werden Ihnen am Ende des Dokumentes zusätzlich in Bildqualität zur Verfügung gestellt.

Mit freundlichen Grüßen
Ihre TIB

IMPORTANT NOTICE

All the pages featuring illustrations have also been made available for you in picture quality at the end of the document.

Many thanks for your understanding,
Your TIB

Monitoring Strain Rate Effects on Nanocomposites using Piezospectroscopy

Erik Durnberg*, Ashley Jones†, Joseangel Rosas‡,
University of Central Florida, Orlando, Florida, USA
George Sunny§
Air Force Research Laboratory, Munitions Directorate, Eglin Air Force Base, USA
Seetha Raghavan ¶
University of Central Florida, Orlando, Florida, USA

Alumina nanoparticles can be added to an epoxy matrix to improve material properties and also allow for the monitoring of stress within the composite. This stress monitoring ability is enabled by the photoluminescent characteristics of alumina. Known as the piezospectroscopic effect, the characteristic R-line peaks present in the emission spectrum of alumina shift with stress. The use of piezospectroscopy to study the effects of strain rates on nanocomposites is a novel approach. In this work, alumina-epoxy nanocomposites of 4.5, 13.6 and 29.7% were investigated under low compressive strain rates of $10^{-4}s^{-1}$, $10^{-3}s^{-1}$ and $10^{-2}s^{-1}$. For each volume fraction and strain rate, the R1 peak shift with respect to applied uniaxial compressive stress was observed. Results illustrate the capability of alumina nanoparticles to act as diagnostic sensors to measure the stress-induced shifts of the spectral R-line peaks under dynamic loading conditions. The range of PS coefficients measured, correlates well in comparison with static experimental behavior for similar volume fractions. Results also show that as the strain rate increases, the failure of the sample was delayed to an increased stress value. Upon further analysis of the data, a general trend of increasing sensitivity of the PS coefficients with increasing strain rate was shown. Also, the dynamic PS coefficients measured here show an increased sensitivity to stress when compared to similar materials under static conditions. This information can be used to determine the time-dependent micro-scale stresses the nanoparticles sustain during composite loading.

Nomenclature

α	alpha phase
l/mm	lines per millimeter
$R1$	Spectral emission peak from alumina
$R2$	Spectral emission peak from alumina
σ_{ij}	piezospectroscopic stress tensor
π_{ij}	piezospectroscopic coefficients
$\delta\nu$	frequency shift
Π_{NC}	nanocomposite piezospectroscopic coefficient
$\sigma_{applied}$	applied nanocomposite stress

*Graduate Student, Mechanical and Aerospace Engineering, AIAA Student Member
†Graduate Student, Mechanical and Aerospace Engineering, AIAA Student Member
‡Undergraduate Student, Mechanical and Aerospace Engineering, AIAA Student Member
§Research Mechanical Engineer, Air Force Research Laboratory, Munitions Directorate
¶Assistant Professor, MAE, UCF, AIAA Associate Fellow, seetha.raghavan@ucf.edu

I. Introduction

THE addition of reinforcing particulates within a polymeric matrix has demonstrated benefits in the overall material properties of the nanocomposite in response to external loading. These nanocomposites exhibit enhanced properties ideal for applications in aerospace and defense. Some examples include light-weight armors that have superior load bearing capability under external impact of blast and energetic materials that have a high amount of energy release with reduced sensitivity to impact. Composites with reinforcing particles can be customized for desired mechanical properties with different matrix or filler materials, particle size, shape, or volume content, and loaded under any condition[1–6]. In addition to the benefit of customization, particulate composites can have improved fatigue resistance, corrosion resistance, and lower manufacturing costs, which make them very attractive when compared to their conventional metal counterparts. Nanometer sized TiO_2 particles in an epoxy matrix have been used to increase composite scratch resistance[7], flexural strength, and toughness[8]. SiC has been used in various matrices to increase the strength of the composite[9], and aluminum particles have been introduced to epoxy to increase fracture toughness[10]. The contrast in rigidities offered by the particles and the matrix has benefits in providing energy dissipating properties which are utilized in applications for protection against micrometeorites for satellites and high-speed particle impact for jet engine turbine blades[11]. Ceramic nanocomposites, specifically, alumina particulate composites are becoming more widely used due to their low densities and relatively high strengths[12]. High stiffness-to-weight ratios due to increased particle rigidity facilitates load transfer to the particles and high surface areas allow for sufficient particle-matrix bonding. Statically, alumina particles have been used in adhesives[13–15] and as plasma sprayed coatings to improve the wear, thermal, electrical, and/or corrosion properties of machine components[16,17]. Dynamic applications of alumina particulate composites include encapsulation of ferroelectric elements for shock depoling[18] and potting compounds for explosive and propellant tests[19,20]. Various types of alumina composites have also been used as armor materials[21], where the durability and energy dissipating properties have proved beneficial.

In addition to improved mechanical properties, chromium doped α-alumina particles can offer additional diagnostic benefits through their photo-luminescent properties. Through the use of optical methods, such as piezospectroscopy, particle stresses and load transfer mechanics can be characterized through the piezospectroscopic (PS) coefficient by measuring the stress-induced shifts of the characteristic R-line peaks present in the emission spectrum of alumina, known as the PS effect. The increased significance of particulate composites such as alumina-epoxy nanocomposites motivates the need to develop these novel measurement techniques to understand the material behavior under static, quasi-static, or dynamic conditions. Previous studies have demonstrated the successful PS calibration of the static response of alumina particulate composites[3,22]. This highlights the potential for this method to monitor particulate stress under variable strain rates in the quasi-static regime, typical in many applications.

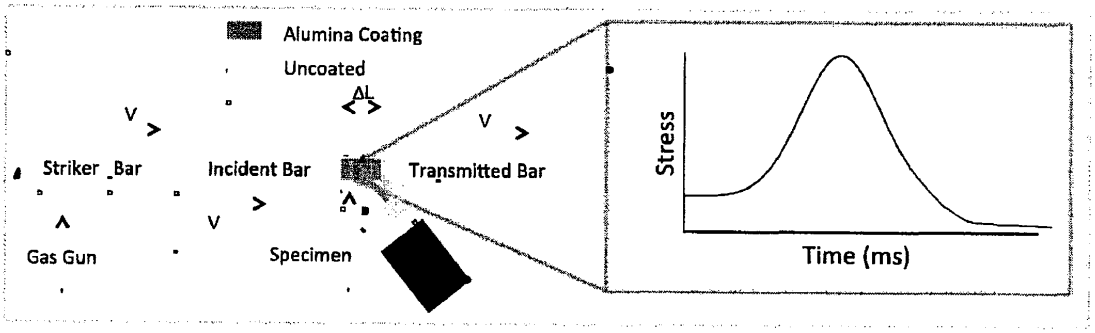

Figure 1: Future application of dynamic piezospectroscopy for possible use in impact testing

One specific application in this regime is stress monitoring in particulate composites during the cure period. When a polymer base, such as an epoxy, is cured, the applied thermal loads cause mechanical loads within the composites. These mechanical loads cause residual stress within the final products, which can affect the overall material properties

of the composite. The novel technique presented here could potentially enable the monitoring of this stress as the composite cures. This information could then be used to cure a composite to a desired residual stress or tailor the curing process as to minimize this residual stress. Additionally, in the ever-expanding field of additive manufacturing, this technique to monitor stress during quasi-static loading can be applied to ensure each layer of material is applied uniformly. As each layer of material cures, the shear stress between the layers could be monitored to avoid stress concentrations in the final composite. In addition to the current applications in static and quasi-static loading regimes, this technique could be applied to dynamic testing in the future. One such future application of this work is shown in Figure 1. There, the stress in the alumina-epoxy coating is being monitored while the test sample undergoes a high strain rate impact from a Split Hopkinson Pressure Bar. The micro-scale stress data collected during the impact could be used to investigate failure mechanics during an impact event on a microscopic scale. The realization of this application is currently only limited by the speed of the spectral data collection system.

It has been shown that this novel technique for stress monitoring can be used in static applications (in previous work), quasi-static applications (in this work) and has significant promise in dynamic regimes. Since the material behavior of composites, those studied in this work and previously, has been shown to vary significantly with strain rate[23], understanding the failure mechanics under variable strain rates is important for the design and safe use of these materials. The need to understand the mechanics of particulate composites, such as alumina-epoxy nanocomposites, coupled with the potential for high speed in-situ collection of stress information of this material using piezospectroscopy provides an excellent motivation for the variable strain rate studies initiated through this work.

II. Experimental Procedure

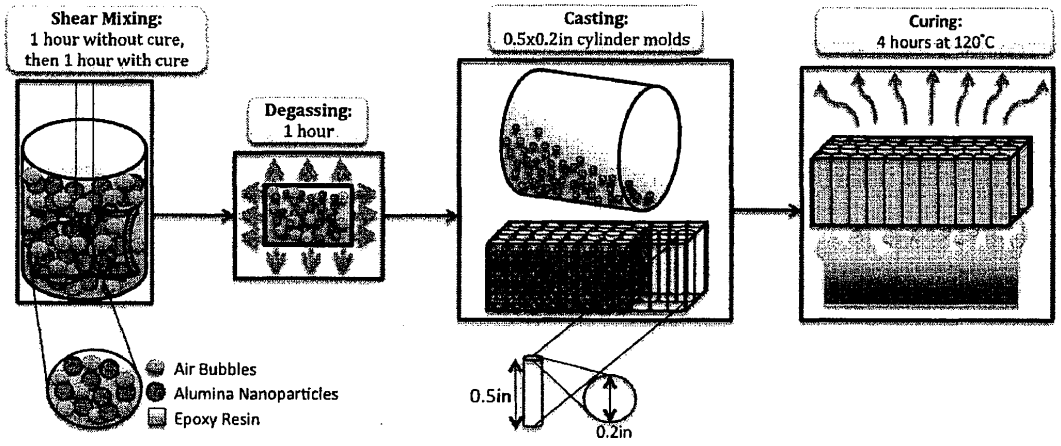

Figure 2: Fabrication of alumina-epoxy composites consisting of shear mixing, degassing, casting, and curing

The bulk alumina-epoxy composites for testing were fabricated using α-alumina nanopowder with an average particle size of 150 nm, 99.85% purity, and a density of 3.97 g/cm^3 as the filler material. The epoxy resin, density of 1.17 g/cm^3, and curing agent implemented was Epon 862 (Bisphenol-F type) and Epikure-W, respectively. Volume fractions were chosen to correlate to static studies[3], which resulted in 4.5, 13.6, and 29.7% in volume of alumina filler material. Appropriate amounts of each component, α-alumina nanoparticles and epoxy resin were measured and mixed using a high shear mixer for a duration of 1 hour as shown in Figure 2. The curing agent was measured and added to the particle-epoxy mixture and mixed for an additional hour. The use of a high shear mixture removed most of the agglomerates that were present, and a low-pressure vacuum system was then utilized for approximately 1 hour to completely remove entrapped air bubbles. The mixture in its uncured state was transferred to a 0.5 in thick aluminum mold with 0.2 in diameter holes. The cast composite was cured for 4 hours in a furnace at 120°C. After the

curing process was complete, the mold was removed from the furnace and the nanocomposite billets were removed while the mold was still warm using a gentle extraction process. Finished sample dimensions were approximately 0.2 in diameter with 0.4 in length. Sample geometry was chosen based upon work by Lankford[24] and Jordan[25] to ensure right cylindrical samples with an aspect ratio of 2:1. Conventional strain gages made from annealed constantan foil with a strain range of up to 20% were also attached and used to collect in-situ strain information with respect to time during loading.

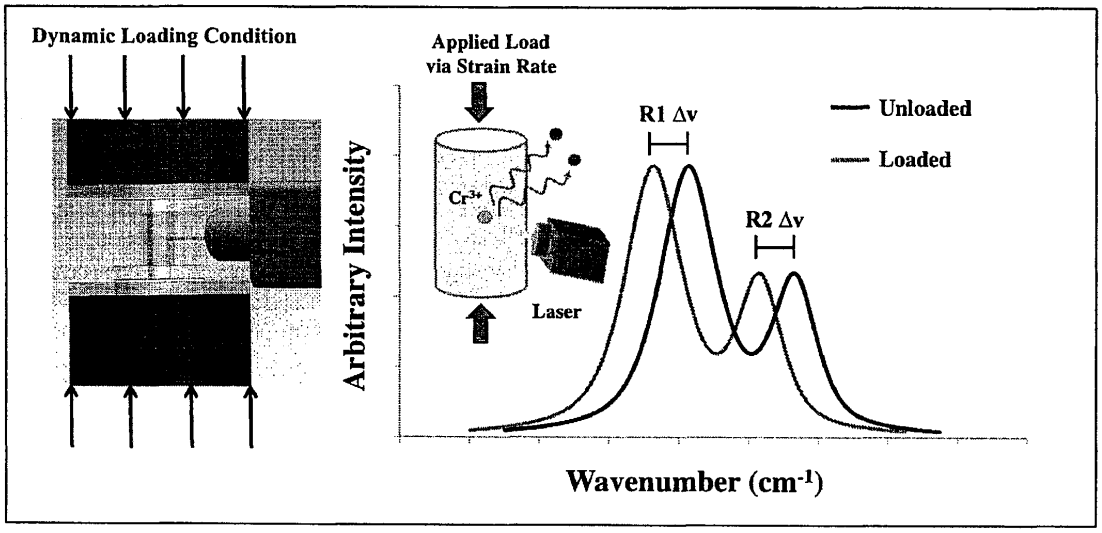

Figure 3: In-situ data collection for PS coefficient determination under quasi-static loading conditions[27]

Table 1: Summary of Samples

# of Samples	Strain Rate
3	$10^{-4}s^{-1}$
3	$10^{-3}s^{-1}$
3	$10^{-2}s^{-1}$

(a) 4.5% Samples

# of Samples	Strain Rate
1	$10^{-4}s^{-1}$
1	$10^{-3}s^{-1}$
1	$10^{-2}s^{-1}$

(b) 13.6% Samples

# of Samples	Strain Rate
3	$10^{-4}s^{-1}$
2	$10^{-3}s^{-1}$
3	$10^{-2}s^{-1}$

(c) 29.7% Samples

The experimental setup was utilized for both mechanical and piezospectroscopic characterization. A Renishaw Raman spectrometer with a 2400 l/mm grating and attached fiber optic probe[26] was used to obtain photo-stimulated luminescent spectroscopy (PSLS) readings. A Ne-Ar source was used to calibrate the spectrometer before data collection. The laser used had an excitation wavelength of 532 nm with approximately 18.5 mW of power at the probe exit. The collection of data is shown in Figure 3 depicting the resulting peaks R1 and R2 and their shift with stress. An MTS Insight Electromechanical system was utilized to apply a stress via crosshead deflection in order to achieve target strain rates of 10^{-4}, 10^{-3}, and $10^{-2}s^{-1}$. The maximum force the sample sustained was recorded using values from the electromechanical test system. This value was divided by the initial sample cross-sectional area and correlated to calculated strain values using data from attached strain gages. The exposure time for PSLS data collection was 0.1 s with 1 accumulation for 4.5 and 29.7% and 0.05 s and 3 accumulations for 13.6% at all rates of loading. The exposure time for each volume fraction was determined in order to allow for sufficient exposure and resulting photo-luminescence, which is needed for sufficient intensities to enable accuracy in R-line peak monitoring, without CCD saturation. A summary of the samples tested in this work is included in Table 1.

III. Results and Discussion

Photo-luminescent data was collected in-situ as shown in Figure 3 and peak position shifts for R1 were analyzed. Due to the similarity between the trends in the R1 and R2 data, only R1 results are presented here. The slope of the peak shift with respect to the applied stress is represented by the piezospectroscopic (PS) coefficient and this coefficient is an indication of the load transfer to the particles. The unloaded R-line peak positions for each sample were used as the reference point to which all subsequent R1 shifts with stress were analyzed. This reference position would also account for any residual stress introduced by the manufacturing process and as a result, the PS coefficients presented in this work are determined with respect to the unloaded sample. Each sample was loaded continuously under compression at the quasi-static strain rates as determined by the attached strain gage.

As each sample was loaded, photo-stimulated luminescent spectroscopy (PSLS) data was taken using the system described. The R1 peak shift was plotted against the applied uniaxial stress for each volume fraction as seen in Figure 4 and Figure 5. The data was smoothed for these plots using a moving average. To quantify the error in the measurements a residual peak shift was calculated at each data point by subtracting the smoothed data point from the actual data point. The average peak shift residual for each sample was calculated. The maximum error observed in the lowest strain rate ($10^{-2}s^{-1}$) data was $\pm 0.0085cm^{-1}$ and in the intermediate strain rate ($10^{-3}s^{-1}$) data was $\pm 0.0097cm^{-1}$. For the highest strain rate of $10^{-2}s^{-1}$, only a few data points were able to be collected in the short span of the test. This caused the resulting R1 peak shift versus stress plots to have very little noise and as a result, the data for that strain rate was not smoothed. With the smoothed data, clearer trends were observed and the strain rate effect was able to be investigated.

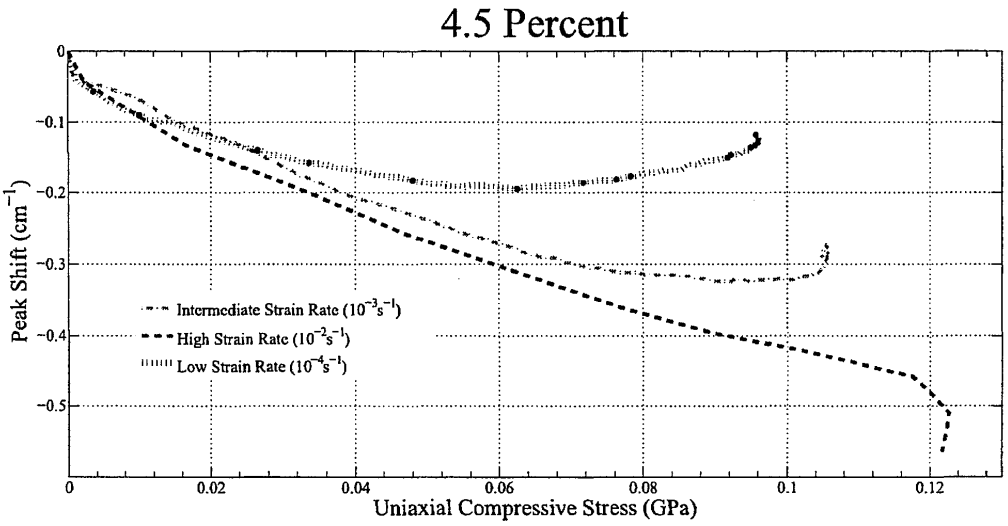

Figure 4: R1 Peak Shift dependence on strain rate for the 4.5% volume fraction

The data for all tested strain rates ($10^{-4}s^{-1}$, $10^{-3}s^{-1}$ and $10^{-2}s^{-1}$) are plotted on the same graph. Figure 4 shows the data for the 4.5% volume fraction samples in which there are clear differences in the behavior of the samples at the three different strain rates. Although all strain rates exhibit similar linear slopes, the failure regions differ significantly for different strain rates. The lowest strain rate data shows failure of the sample is starting around $0.065GPa$, with failure beginning for the intermediate strain rate at $0.085GPa$, and failure starting to occur in the highest strain rate data at $0.115GPa$. It is clear that increasing the strain rate delays the failure of the sample, and increases the ultimate compressive strength of the sample. A similar trend to the 4.5% samples can be seen with the 13.6% samples, shown in Figure 5, however, a failure region for the high strain rate data was not observed due to the speed of the test and

the limitations of the data collection hardware. Lastly, Figure 5 shows the data for the 29.7% samples. Here, the trend of increasing strength with increasing strain rate is observed again for the entire range of strain rates tested. As with the 4.5% samples, the high strain rate data shows details of a region of increased stress sensitivity. Overall, Figure 4 and Figure 5 show that, independent of volume fraction, as the strain rate is increased, the onset of sample failure is postponed to higher stress values.

Insight into the stress transferred to the particles in the alumina-epoxy composites during failure is also apparent in Figure 4 and Figure 5. It can be seen that for the low and mid range strain rates, once a peak magnitude for the R1 peak shift is attained, the samples go through a period of decreased stress transfer to the particle. This can be interpreted as the overall stress in the composite increasing and the stress transferred to the alumina particles decreasing. This same pattern can be seen across all volume fractions, 4.5, 13.6 and 29.7%. The opposite behavior is seen for the high strain rate data for both the 4.5% and 29.7% volume fractions; as the stress in the overall sample increases past a certain value, increased stress sensitivity in the particles is observed. This indicates that the particles are absorbing more stress from the composite as higher loads are achieved. A similar trend may be present in the high strain rate data for the 13.6% samples; however, the high speeds of the test and hardware limitations may have contributed to the absence of a transition period for those samples.

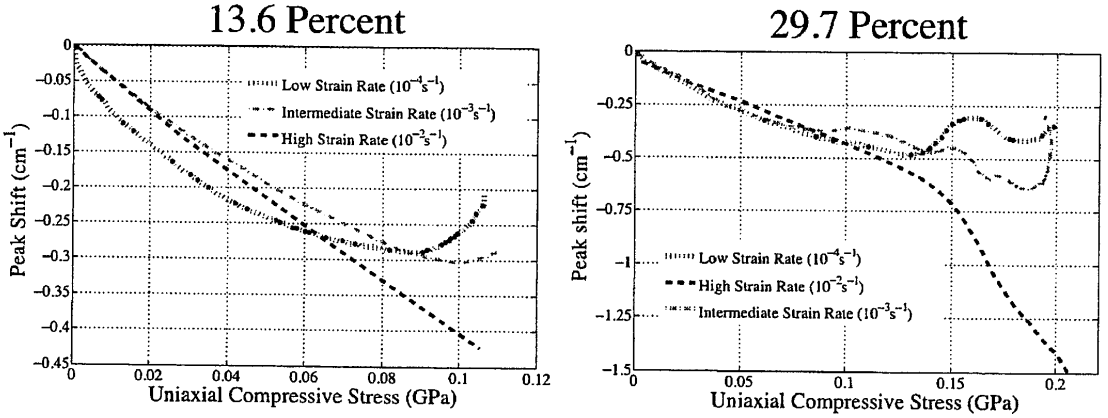

Figure 5: R1 Peak Shift dependence on strain rate for the 13.6% and 29.7% volume fractions

Higher volume fractions of alumina-epoxy composites are generally more difficult to manufacture and issues such as completely dispersing the filler material in the matrix could lead to the presence of agglomerations and voids within the sample. Regions that are not completely homogeneous could cause localized stress concentrations within the sample, resulting in an uneven stress distribution and poor load transfer mechanics. Stress concentrations within the sample would cause the sample to fail prematurely or have high stresses in regions other than the data collection location, thus leading to inaccurate values of PS coefficient sensitivity. In addition to the manufacturing difficulties, higher volume fraction samples inherently have more particles and less matrix material. As a result, there is less binding material within the sample and higher concentrations of ceramic particles, which may also affect the stress distribution of the sample at the microscale. The uncharacteristic and unpredictable fluctuations in the 29.7% data shown in Figure 5 can be attributed to the combination of all these factors.

To determine the relationship between volume fraction and stress sensitivity, the R1 peak shift for all volume fractions was plotted against stress. The failure region is highly dependent on difficult to control variables such as sample manufacturing and sample dimensions. As a result, to avoid including the unpredictable failure regime in these studies, the data presented accounts for only the linear part of the stress-strain curve. For the low range of strain rates around $10^{-4}s^{-1}$, the data set was very large and noisy, which resulted in data that was only qualitative. The opposite was true for the high range of strain rates around $10^{-2}s^{-1}$. Due to the limited amount of data (a result of the high

speed nature of the tests) these tests were only useful for qualitative purposes. As a result, only the intermediate strain rates were considered for the PS coefficient studies presented here.

Table 2: Dynamic and Static PS coefficient comparison

Quasi-Static PS Coefficient (Volume Fraction)	Static PS Coefficient[3] (Volume Fraction)
$-4.16cm^{-1}/GPa$ (4.5%)	$-3.16cm^{-1}/GPa$ (5%)
$-4.29cm^{-1}/GPa$ (13.6%)	$-3.34cm^{-1}/GPa$ (20%)
$-4.88cm^{-1}/GPa$ (29.7%)	$-4.10cm^{-1}/GPa$ (34%)

Table 2 shows the dynamic PS coefficients compared to static PS coefficients of similar volume fractions. Note that the tabulated values are for the intermediate strain rate of $10^{-3}s^{-1}$, as previously mentioned. The dynamic PS coefficients listed were calculated using only the linear portion of the R1 peak shift versus stress plots. The linear portion was identified by using the stress strain curves for each sample to determine the stress at which sample yielding started to occur. One such curve, for a 4.5% volume fraction sample tested at the intermediate strain rate of $10^{-3}s^{-1}$, is shown in Figure 6. It is evident that the dynamic PS coefficients listed increased with increasing volume fraction, as 4.5% has the lowest magnitude R1 PS coefficient of $-4.16cm^{-1}/GPa$, 13.6% has a R1 PS coefficient of $-4.29cm{-}1/GPa$, and 29.7% has the highest magnitude R1 PS coefficient of $-4.88cm^{-1}/GPa$. This trend of increasing PS coefficient with volume fraction is also seen in static data[3] for comparable volume fractions. The static data[3] is presented in Table 2 as well and shows the quasi-static PS coefficients presented here are consistently greater than the comparable static PS coefficients. This indicates that the higher volume fraction alumina-epoxy composites are more sensitive to stress than lower volume faction alumina-epoxy composites, even during quasi-static loading events. The increase in PS coefficient for the quasi-static tests indicate that the PS coefficients for these composites are dependent on strain rate and that as the strain rate is increased, the composites sensitivity to stress also increases. The increased PS coefficients observed here signify an increase in the stress resolution of this technique under quasi-static conditions when compared to previous static experiments[3].

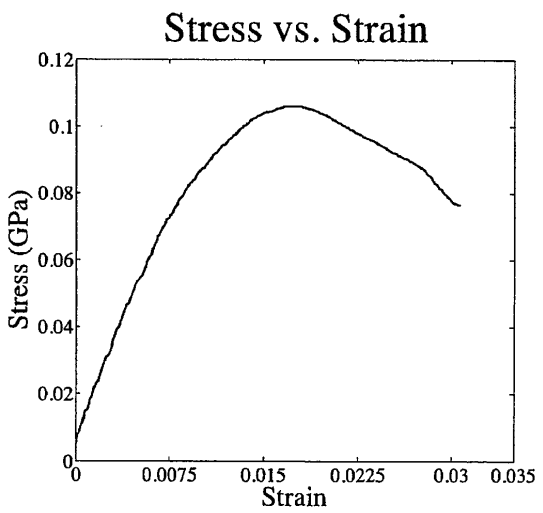

Figure 6: Stress-Strain curve for a 4.5% sample tested at a strain rate of $10^{-3}s^{-1}$

While the stress sensitivity was expected to increase with increasing strain rate, the complex microscale factors ultimately have a large influence on the PS sensitivity results and made it difficult to show that expectation. Factors such as microcracking are most certainly affected by increasing strain rates, which affect the degree of load transfer to the particle modifiers and thus affect the PS sensitivity. Factors such as particle dispersion, which varies for each sample, also affect the PS sensitivity. In order to minimize the affects of these issues on this work, relatively low strain rates were used, and particle dispersion studies were conducted for every sample. The dispersion tests were done at zero load for each sample and consisted of a vertical PSLS scan to show the varying intensity, which is indicative of varying alumina particle concentrations. With this data, the samples that had the best dispersion were chosen to be the most representative of a specific volume fraction because they exhibited the least amount of localized volume fraction variation. By mitigating as many factors as possible, the particle behavior in relation to strain rate was ultimately determined, and it was clearly shown in this work that the loading rate does have an impact on the load transfer and the resulting PS sensitivity.

IV. Conclusion

The results illustrate the capability of alumina nanoparticles to act as diagnostic sensors to measure the stress-induced shifts of the spectral R-line peaks resulting from stress applied by low compressive strain rates. The range of R1 PS coefficients measured, -4.16 to $-4.88cm^{-1}/GPa$, show some variation from previous static test results of similar volume fractions, -3.16 to $-4.10cm^{-1}/GPa$; however the same trend of increasing PS coefficients with increasing volume fraction is seen in both the quasi-static and static data. In addition, the magnitude of the PS coefficients for a given strain rate are consistently greater than the magnitude of the PS coefficients for comparable static tests. This supports the expectation that during quasi-static loading events, the compressive strength of the composite increases. Results also reveal that, independent of volume fraction, the alumina-epoxy nanocomposites exhibit delayed failure with respect to stress as the strain rate is increased. This result illustrates the improved composite performance under increased strain rates, which is expected in these types of materials.Improvements in composite dispersion, especially at higher volume fractions, may lend to improved stress distributions within the sample and improved curve fitting techniques may lend to more accurate R-line peak position shifts. Calibration of the in-situ diagnostic stress-sensing capabilities of varying volume fractions of alumina-epoxy nanocomposites under quasi-static strain rates in this work set the precedent for future studies at high strain rates.

Acknowledgments

This work is supported by the University of Central Florida In-house Research Grant and National Science Foundation Graduate Research Fellowship under Grant No. DGE-1144246.

References

[1]Jordan, J., White, B., Spowart, J., Thadhani, N., and Richards, D., "Static and dynamic mechanical properties of epoxy-based multi-constituent particulate composites," *DYMAT 2009 - 9th International Conferences on the Mechanical and Physical Behaviour of Materials under Dynamic Loading*, DYMAT, 2009, pp. 19–25.

[2]Shukla, D. K. and Parameswaran, V., "Epoxy composites with 200 nm thick alumina platelets as reinforcements," *Journal of Material Science*, Vol. 42, 2007, pp. 5964–5972.

[3]Stevenson, A., *Calibration of Alumina-Epoxy Nanocomposites using Piezospectroscopy for the Development of Stress-Sensing Adhesives*, Master's thesis, University of Central Florida, 2011.

[4]Stevenson, A., Jones, A., and Raghavan, S., "Characterization of particle dispersion and volume fraction in alumina-filled epoxy nanocomposites using photo-stimulated luminescence spectroscopy," *Polymer*, Vol. 43, 2011, pp. 17.

[5]Bhimaraj, P., Burris, D. L., Action, J., Sawyer, W. G., Toney, C. G., Siegel, R. W., and Schadler, L. S., "Effect of matrix morphology on the wear and friction behavior of alumina nanoparticle/poly(ethylene) terephthalate composites," *Wear*, Vol. 258, 2005, pp. 1437–1443.

[6]Chisholm, N., Mahfuz, H., Rangari, V. K., Ashfaq, A., and Jeelani, S., "Fabrication and mechanical characterization of carbon/SiC-epoxy nanocomposites," *Composite Structures*, Vol. 67, 2005, pp. 115–124.

[7]Ng, C., Scbadler, L., and Siegel, R., "Synthesis and Mechanical Properties of TiO_2-Epoxy Nanocomposites," *NanoStructured Materials*, Vol. 12, 1999, pp. 507–510.

[8]Wetzel, B., Rosso, P., Haupert, F., and Friedrich, K., "Epoxy nanocomposites - fracture and toughening mechanisms," *Engineering Fracture Mechanics*, Vol. 73, 2006, pp. 2375–2398.

[9]Derby, B., "Ceramic nanocomposites: mechanical properties," *Current Opinion in Solid State and Materials Science*, Vol. 3, 1998, pp. 490–495.

[10]Zunjarrao, S. C. and Singh, R. P., "Characterization of the fracture behavior of epoxy reinforced with nanometer and micrometer sized aluminum particles," *Composites Science and Technology*, Vol. 66, 2006, pp. 2296–2305.

[11]Lee, J. H., Veysset, D., Singer, J. P., Retsch, M., Saini, G., Pezeril, T., Nelson, K. A., and Thomas, E. L., "High strain rate deformation of layered nanocomposites," *Nature Communications*, Vol. 3, 2012, pp. 1164.

[12]Jordan, J. L., Ferranti, L., Austin, R. A., Dick, R. D., Foley, J. R., Thadhani, N. N., McDowell, D. L., and Benson, D. J., "Equation of state of aluminum-iron oxide-epoxy composite," *Journal of Applied Physics*, Vol. 101, No. 093520, 2007, pp. 1–9.

[13]Gilbert, E. N., Hayes, B. S., and Seferis, J. C., "Nano-alumina modified epoxy based film adhesives," *Polymer Engineering and Science*, Vol. 43, May 2003, pp. 1096–1104.

[14]Lee, D. G., Kim, J. K., and Cho, D. H., "Effects of adhesive fillers on the strength of tubular single lap adhesive joints," *Journal of Adhesion Science Techonology*, Vol. 13, 1999, pp. 1343–1360.

[15]Dorigato, A. and Pegoretti, A., "The role of alumina nanoparticles in epoxy adhesives," *Journal of Nanoparticle Research*, Vol. 13, 2011, pp. 2429–2441.

[16]Erickson, L. C., Troczynski, T., Hawthorne, H. M., Tai, H., and Ross, D., "Alumina Coatings by Plasma Spraying of Monosize Sapphire Particles," *Journal of Thermal Spray Technology*, Vol. 8, 1999, pp. 421–426.

[17]Xu, Z. H. and Rowcliffe, D., "Nanoindentation on diamond-like carbon and alumina coatings," *Surface and Coatings Technology*, Vol. 161, 2002, pp. 44–51.

[18]Lysne, P. C. and Percival, C. M., "Electric energy generation by shock compression of ferroelectric ceramics: Normal-mode response of PZT 95/5," *Journal of Applied Physics*, Vol. 46, 1975, pp. 1519–1525.

[19]Millett, J. C. F., Bourne, N. K., and Deas, D., "The equation of state of two alumina-filled epoxy resins," *Journal of Physics D: Applied Physics*, Vol. 38, 2005, pp. 930–934.

[20]Drumheller, D. S., "On the dynamical response of particulate loaded materials. II. A theory with application to alumina particles in an epoxy matrix," *Journal of Applied Physics*, Vol. 53, 1982, pp. 957–969.

[21]Dancer, C., Curtis, H., Bennett, S., Petrinic, N., and Todd, R., "High strain rate indentation-induced deformation in alumina ceramics measured by Cr^{3+} fluorescence mapping," *Journal of the European Ceramic Society*, Vol. 31, 2011, pp. 2177–2187.

[22]Stevenson, A., Jones, A., and Raghavan, S., "Stress-Sensing Nanomaterial Calibrated with Photostimulated Luminescence Emission," *Nano Letters*, Vol. 11, 2011, pp. 3274–3278.

[23]Jacob, G. C., Starbuck, J. M., Fellers, J. F., Simunovic, S., and Boeman, R. G., "Strain Rate Effects on the Mechanical Properties of Polymer Composite Materials," *Journal of Applied Polymer Science*, Vol. 94, 2004, pp. 296–301.

[24]Lankford, J., "Compressive strength and microplasticity in polycrystalline alumina," *Journal of Materials Science*, Vol. 12, 1977, pp. 791–796.

[25]Jordan, J. L., Foley, J. R., and Siviour, C. R., "Mechanical properties of Epon 826/DEA epoxy," *Mech Time-Depend Mater*, Vol. 12, 2008, pp. 249–272.

[26]Freihofer, G., Poliah, L., Walker, K., Medina, A., and Raghavan, S., "Optical stress probe: In situ stress mapping with raman and photo-stimulated luminescence spectroscopy," *Journal of Instrumentation*, Vol. 5, 2010.

[27]Jones, A., *Low Strain Rate Studies of Alumina-Epoxy Composites using Piezospectroscopy*, Master's thesis, University of Central Florida, 2013.

I. Introduction

THE addition of reinforcing particulates within a polymeric matrix has demonstrated benefits in the overall material properties of the nanocomposite in response to external loading. These nanocomposites exhibit enhanced properties ideal for applications in aerospace and defense. Some examples include light-weight armors that have superior load bearing capability under external impact of blast and energetic materials that have a high amount of energy release with reduced sensitivity to impact. Composites with reinforcing particles can be customized for desired mechanical properties with different matrix or filler materials, particle size, shape, or volume content, and loaded under any condition [1–6]. In addition to the benefit of customization, particulate composites can have improved fatigue resistance, corrosion resistance, and lower manufacturing costs, which make them very attractive when compared to their conventional metal counterparts. Nanometer-sized TiO_2 particles in an epoxy matrix have been used to increase composite scratch resistance[7], flexural strength, and toughness[8]. SiC has been used in various matrices to increase the strength of the composite[9], and aluminum particles have been introduced to epoxy to increase fracture toughness[10]. The contrast in rigidities offered by the particles and the matrix has benefits in providing energy dissipating properties which are utilized in applications for protection against micrometeorites for satellites and high-speed particle impact for jet engine turbine blades[11]. Ceramic nanocomposites, specifically, alumina particulate composites are becoming more widely used due to their low densities and relatively high strengths[12]. High stiffness-to-weight ratios due to increased particle rigidity facilitates load transfer to the particles and high surface areas allow for sufficient particle-matrix bonding. Statically, alumina particles have been used in adhesives[13–15] and as plasma sprayed coatings to improve the wear, thermal, electrical, and/or corrosion properties of machine components[16,17]. Dynamic applications of alumina particulate composites include encapsulation of ferroelectric elements for shock depoling[18] and potting compounds for explosive and propellant tests[19,20]. Various types of alumina composites have also been used as armor materials[21], where the durability and energy dissipating properties have proved beneficial.

In addition to improved mechanical properties, chromium doped α-alumina particles can offer additional diagnostic benefits through their photo-luminescent properties. Through the use of optical methods, such as piezospectroscopy, particle stresses and load transfer mechanics can be characterized through the piezospectroscopic (PS) coefficient by measuring the stress induced shifts of the characteristic R-line peaks present in the emission spectrum of alumina, known as the PS effect. The increased significance of particulate composites such as alumina-epoxy nanocomposites motivates the need to develop these novel measurement techniques to understand the material behavior under static, quasi-static, or dynamic conditions. Previous studies have demonstrated the successful PS calibration of the static response of alumina particulate composites[7,22]. This highlights the potential for this method to monitor particulate stress under variable strain rates in the quasi-static regime, typical in many applications.

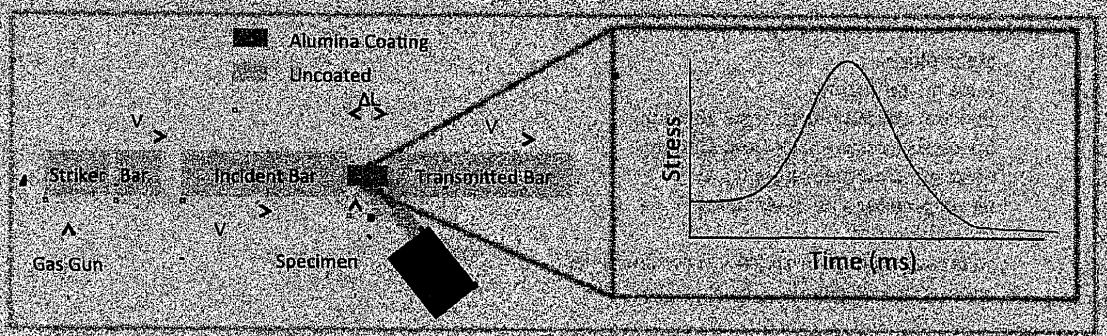

Figure 1: Future application of dynamic piezospectroscopy for possible use in impact testing.

One specific application in this regime is stress monitoring in particulate composites during the cure period. When a polymer base, such as an epoxy, is cured, the applied thermal loads cause mechanical loads within the composites. These mechanical loads cause residual stress within the final products, which can affect the overall material properties

of the composite. The novel technique presented here could potentially enable the monitoring of this stress as the composite cures. This information could then be used to cure a composite to a desired residual stress or tailor the curing process as to minimize this residual stress. Additionally, in the ever-expanding field of additive manufacturing, this technique to monitor stress during quasi-static loading can be applied to ensure each layer of material is applied uniformly. As each layer of material cures, the shear stress between the layers could be monitored to avoid stress concentrations in the final composite. In addition to the current applications in static and quasi-static loading regimes, this technique could be applied to dynamic testing in the future. One such future application of this work is shown in Figure 1. There, the stress in the alumina-epoxy coating is being monitored while the test sample undergoes a high strain rate impact from a Split Hopkinson Pressure Bar. The micro-scale stress data collected during the impact could be used to investigate failure mechanics during an impact event on a microscopic scale. The realization of this application is currently only limited by the speed of the spectral data collection system.

It has been shown that this novel technique for stress monitoring can be used in static applications (in previous work), quasi-static applications (in this work) and has significant promise in dynamic regimes. Since the material behavior of composites, those studied in this work and previously, has been shown to vary significantly with strain rate[23], understanding the failure mechanics under variable strain rates is important for the design and safe use of these materials. The need to understand the mechanics of particulate composites, such as alumina-epoxy nanoComposites, coupled with the potential for high speed in situ collection of stress information of this material using piezospectroscopy provides an excellent motivation for the variable strain rate studies initiated through this work.

II. Experimental Procedure

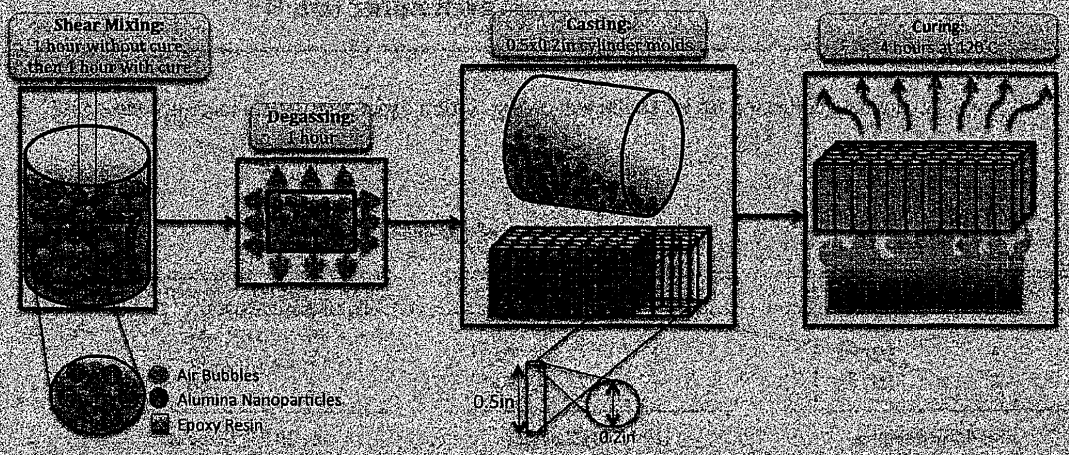

Figure 2. Fabrication of alumina-epoxy composites consisting of shear mixing, degassing, casting, and curing.

The bulk alumina-epoxy composites for testing were fabricated using α-alumina nanopowder with an average particle size of 150 nm, 99.85% purity, and a density of 3.97 g/cm^3 as the filler material. The epoxy resin, density of 1.17 g/cm^3, and curing agent implemented was Epon 862 (Bisphenol-F type) and Epikure-W, respectively. Volume fractions were chosen to correlate to static studies[23], which resulted in 4.5, 13.6, and 29.7% in volume of alumina filler material. Appropriate amounts of each component, α-alumina nanoparticles and epoxy resin, were measured and mixed using a high shear mixer for a duration of 1 hour as shown in Figure 2. The curing agent was measured and added to the particle-epoxy mixture and mixed for an additional hour. The use of a high shear mixture removed most of the agglomerates that were present, and a low-pressure vacuum system was then utilized for approximately 1 hour to completely remove entrapped air bubbles. The mixture in its uncured state was transferred to a 0.5 in thick aluminum mold with 0.2 in diameter holes. The cast composite was cured for 4 hours in a furnace at 120° C. After the

curing process was complete, the mold was removed from the furnace and the nanocomposite billets were removed while the mold was still warm using a gentle extraction process. Finished sample dimensions were approximately 0.2 *in* diameter with 0.4 *in* length. Sample geometry was chosen based upon work by Lankford[24] and Jordan[25] to ensure right cylindrical samples with an aspect ratio of 2:1. Conventional strain gages made from annealed constantan foil with a strain range of up to 20% were also attached and used to collect in-situ strain information with respect to time during loading.

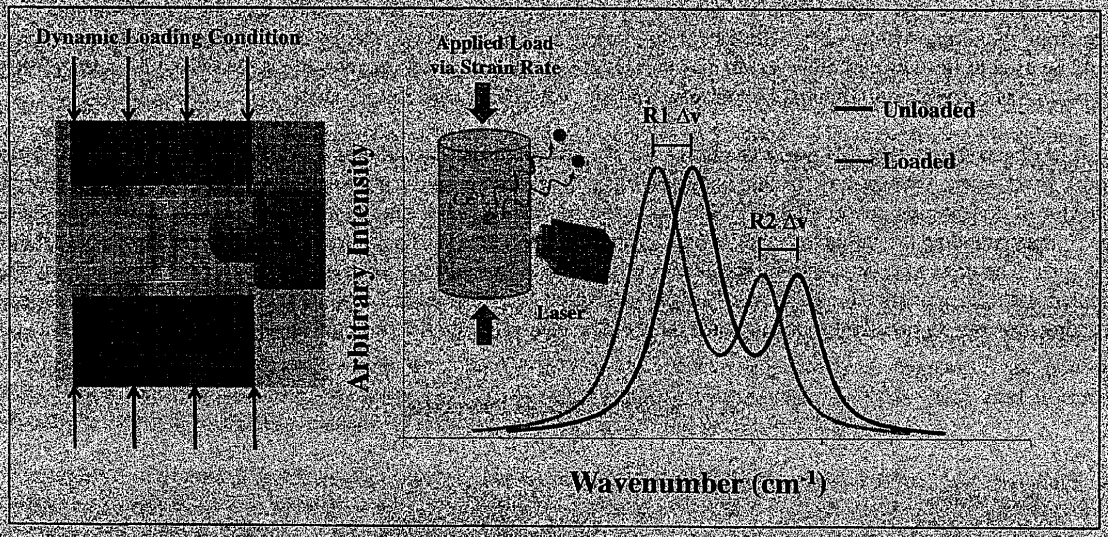

Figure 3: In-situ data collection for PS coefficient determination under quasi-static loading conditions[27]

Table 1: Summary of Samples

# of Samples	Strain Rate
3	$10^{-4}s^{-1}$
3	$10^{-3}s^{-1}$
3	$10^{-2}s^{-1}$

(a) 4.5% Samples

# of Samples	Strain Rate
1	$10^{-4}s^{-1}$
1	$10^{-3}s^{-1}$
1	$10^{-2}s^{-1}$

(b) 13.6% Samples

# of Samples	Strain Rate
3	$10^{-4}s^{-1}$
2	$10^{-3}s^{-1}$
3	$10^{-2}s^{-1}$

(c) 29.7% Samples

The experimental setup was utilized for both mechanical and piezospectroscopic characterization. A Renishaw Raman spectrometer with a 2400 *l/mm* grating and attached fiber optic probe[26] was used to obtain photo-stimulated luminescent spectroscopy (PSLS) readings. A Ne-Ar source was used to calibrate the spectrometer before data collection. The laser used had an excitation wavelength of 532 *nm* with approximately 18.5 *mW* of power at the probe exit. The collection of data is shown in Figure 3 depicting the resulting peaks R1 and R2 and their shift with stress. An MTS Insight Electromechanical system was utilized to apply a stress via crosshead deflection in order to achieve target strain rates of 10^{-4}, 10^{-3}, and $10^{-2}s^{-1}$. The maximum force the sample sustained was recorded using values from the electromechanical test system. This value was divided by the initial sample cross-sectional area and correlated to calculated strain values using data from attached strain gages. The exposure time for PSLS data collection was 0.1 *s* with 1 accumulation for 4.5 and 29.7% and 0.05 *s* and 3 accumulations for 13.6% at all rates of loading. The exposure time for each volume fraction was determined in order to allow for sufficient exposure and resulting photo-luminescence, which is needed for sufficient intensities to enable accuracy in R-line peak monitoring, without CCD saturation. A summary of the samples tested in this work is included in Table 1.

III. Results and Discussion

Photo-luminescent data was collected in-situ as shown in Figure 3 and peak position shifts for R1 were analyzed. Due to the similarity between the trends in the R1 and R2 data, only R1 results are presented here. The slope of the peak shift with respect to the applied stress is represented by the piezospectroscopic (PS) coefficient and this coefficient is an indication of the load transfer to the particles. The unloaded R-line peak positions for each sample were used as the reference point to which all subsequent R1 shifts with stress were analyzed. This reference position would also account for any residual stress introduced by the manufacturing process and as a result, the PS coefficients presented in this work are determined with respect to the unloaded sample. Each sample was loaded continuously under compression at the quasi-static strain rates as determined by the attached strain gage.

As each sample was loaded, photo-stimulated luminescent spectroscopy (PSLS) data was taken using the system described. The R1 peak shift was plotted against the applied uniaxial stress for each volume fraction as seen in Figure 4 and Figure 5. The data was smoothed for these plots using a moving average. To quantify the error in the measurements a residual peak shift was calculated at each data point by subtracting the smoothed data point from the actual data point. The average peak shift residual for each sample was calculated. The maximum error observed in the lowest strain rate ($10^{-2}s^{-1}$) data was $\pm 0.0085cm^{-1}$ and in the intermediate strain rate ($10^{-3}s^{-1}$) data was $\pm 0.0097cm^{-1}$. For the highest strain rate of $10^{-2}s^{-1}$, only a few data points were able to be collected in the short span of the test. This caused the resulting R1 peak shift versus stress plots to have very little noise and as a result, the data for that strain rate was not smoothed. With the smoothed data, clearer trends were observed and the strain rate effect was able to be investigated.

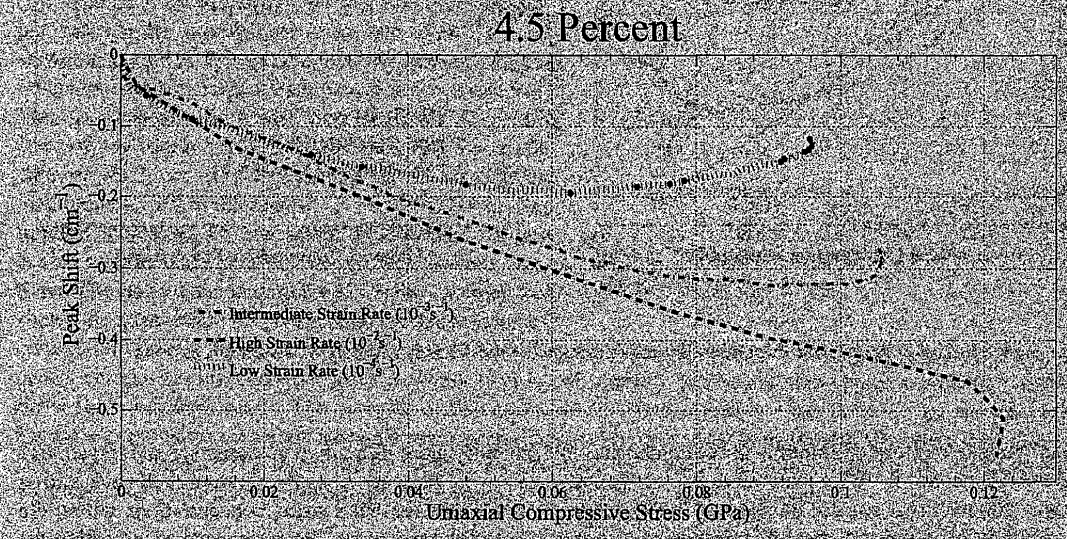

Figure 4. R1 Peak Shift dependence on strain rate for the 4.5% volume fraction

The data for all tested strain rates ($10^{-4}s^{-1}$, $10^{-3}s^{-1}$ and $10^{-2}s^{-1}$) are plotted on the same graph. Figure 4 shows the data for the 4.5% volume fraction samples in which there are clear differences in the behavior of the samples at the three different strain rates. Although all strain rates exhibit similar linear slopes, the failure regions differ significantly for different strain rates. The lowest strain rate data shows failure of the sample is starting around $0.065GPa$, with failure beginning for the intermediate strain rate at $0.085GPa$, and failure starting to occur in the highest strain rate data at $0.115GPa$. It is clear that increasing the strain rate delays the failure of the sample, and increases the ultimate compressive strength of the sample. A similar trend to the 4.5% samples can be seen with the 13.6% samples, shown in Figure 5, however, a failure region for the high strain rate data was not observed due to the speed of the test and